

The NJL model of dense three-flavor matter with axial anomaly: the low temperature critical point and BEC-BCS diquark crossover

Hiroaki Abuki¹, Gordon Baym², Tetsuo Hatsuda³, and Naoki Yamamoto³

¹*Department of Physics, Tokyo University of Science, Tokyo 162-8601, Japan*

²*Department of Physics, University of Illinois, 1110 W. Green St., Urbana, Illinois 61801, USA, and*

³*Department of Physics, The University of Tokyo, Tokyo 113-0033, Japan*

(Dated: November 2, 2018)

We study the QCD phase structure in the three-flavor Nambu–Jona-Lasinio model, incorporating the interplay between the chiral and diquark condensates induced by the axial anomaly. We demonstrate that for an appropriate range of parameters of the model, the interplay leads to the low temperature critical point in the phase structure predicted by a previous Ginzburg–Landau analysis. We also show that a Bose–Einstein condensate (BEC) of diquark molecules emerges in the intermediate density region, and as a result, a BEC–BCS crossover is realized with increasing quark chemical potential.

PACS numbers: 12.38.Aw, 11.10.Wx, 11.30.Rd, 03.75.Nt

I. INTRODUCTION

The phases of strongly interacting matter described by quantum chromodynamics (QCD) at finite temperature T and quark chemical potential μ is being actively studied theoretically, as well as experimentally in ultrarelativistic heavy ion collisions at RHIC (Relativistic Heavy Ion Collider) and in the near future at the LHC (Large Hadron Collider). At low T and μ , the hadronic phase is realized with chiral symmetry dynamically broken by condensation of quark-antiquark pairs, the chiral condensate $\langle \bar{q}q \rangle$. On the other hand, at low T and high μ a color superconducting (CSC) phase [1], characterized by formation of quark-quark pairs – a diquark condensate $\langle qq \rangle$ – is expected to appear owing to the attractive one-gluon exchange interaction or the instanton-induced interaction in the quark-quark channel. At high T for any μ , the quark-gluon plasma (QGP) phase [2] is realized with both the chiral and diquark condensates melted away. The phase transition from the hadronic phase to the QGP phase is indeed confirmed by recent lattice QCD Monte Carlo simulations indicating a smooth crossover for physical quark masses [3, 4].

Nevertheless, the first-principles lattice technique based on importance sampling is not applicable to QCD at finite μ due to the complex fermion determinant. This is why our understanding of the transition from the hadronic phase to the CSC phase relevant to the compact star physics is still immature and we have to basically rely on specific models of QCD, such as the Nambu–Jona-Lasinio (NJL) model [5, 6], the Polyakov–Nambu–Jona-Lasinio (PNJL) model [7–10], and the random matrix theory (RMT) [11–13]. These model studies together with the lattice QCD results have revealed the possible existence of the critical point [14, 15] at high T between the hadronic phase and the QGP phase (see, however, [16]).

Recently, we have pointed out the possibility of a new low temperature critical point between the hadron phase and the CSC phase in three-flavor QCD, on the ba-

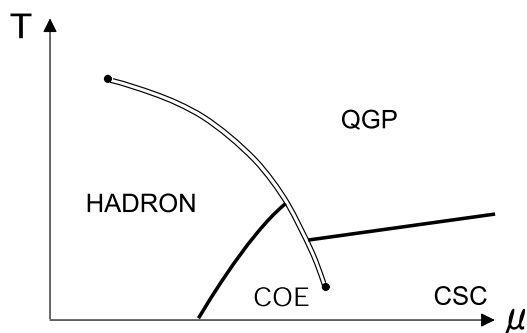


FIG. 1. Schematic phase structure with two light (up and down) quarks and a medium heavy (strange) quark. In the hadronic phase, $q\bar{q}$ pairs condense, while in the color superconducting (CSC) phase, the dominant condensation is qq pairing. In the quark-gluon plasma (QGP), all symmetries are restored without any pairing, while in the coexistence (COE) region $q\bar{q}$ and qq pairings coexist. The double line denotes a first-order phase transition. Adapted from Ref. [18].

sis of model-independent Ginzburg–Landau (GL) theory [17, 18]: the attraction between the chiral and diquark condensates induced by the axial anomaly leads to this critical point and an associated smooth crossover. Figure 1 illustrates the dense three-flavor QCD phase diagram with the new critical point at low T [18]. This may provide a mechanism of continuity between hadronic matter and quark matter (hadron-quark continuity) conjectured by Schäfer and Wilczek [19]. Moreover, the idea of hadron-quark continuity is corroborated by recent studies on the spectral continuity of Nambu–Goldstone modes [18] and vector mesons [20], and the formal similarity of the partition functions in the universal regime between the low and high μ regimes in three-flavor QCD at finite size, large compared with the inverse gap, but small compared with the pion Compton wavelength [21]. In two-flavor QCD, similar new critical points have also been found in the NJL model [22–24], although their origin is related to a repulsive vector-channel four-fermion interaction [22], or electric charge neutrality and

β -equilibrium conditions [23, 24] rather than the axial anomaly. These studies may imply smooth crossovers not only as a function of T at low μ but also as a function of μ at low T in the realistic QCD phase diagram.

The Ginzburg-Landau analysis for three-flavor QCD in Refs. [17, 18] depends on the assumption that the magnitudes of the chiral and diquark condensates are sufficiently small near the phase boundaries, which may not be justified over the entire region in the QCD phase diagram and for strongly first-order phase transitions. The question is unanswered as to whether such a new critical point induced by the axial anomaly does really emerge in the (μ, T) -plane within the framework of phenomenological models with reasonable parameters.

The purposes of this paper are two-fold. First, using the three-flavor NJL model incorporating the interplay between the chiral and diquark condensates induced by the axial anomaly, we study the location of the new critical point predicted in [17, 18]. We demonstrate that this critical point indeed appears in the phase diagram for an appropriate range of parameters. Second, we show that the axial anomaly also triggers, in this model, a crossover between a Bose-Einstein condensed state (BEC) of diquark pairing and Bardeen-Cooper-Schrieffer (BCS) diquark pairing. This BEC-BCS crossover is identical in structure to that in nonrelativistic condensed matter systems [25–27]; and is discussed for relativistic systems [28–37]: the change in size of Cooper pairs at lower μ within the QCD Schwinger-Dyson approach [28], the relativistic BEC-BCS crossover of diquark pairing in the NJL-type model [29, 31, 33–36] and the diquark-quark model [30, 32], and a possible evolution from baryons in nuclear matter to diquarks in quark matter with increasing μ [37] are elucidated. Remarkably, as we will show in this paper, in relativistic quark matter at high μ the axial anomaly enhances the attractive interaction between quarks, leading to the emergence of a BEC state of diquark pairing.

To illustrate the essential physics induced by the axial anomaly and to avoid complications of charge neutrality and β -equilibrium conditions, we assume SU(3) flavor symmetry $m_u = m_d = m_s \equiv m_q$ throughout this paper. The generalization to include these effects will be reported elsewhere.

This paper is organized as follows. In Sec. II, we formulate the three-flavor NJL model incorporating the interplay between the chiral and diquark condensates induced by the axial anomaly. In Sec. III, we discuss the phase structures with and without the interplay. In Sec. IV, we show that the interplay leads not only to the new critical point but also to the BEC-BCS crossover of the diquark pairing at high density. Sec. V is devoted to a summary and concluding remarks.

II. NJL MODEL WITH AXIAL ANOMALY

The Lagrangian of the Nambu–Jona-Lasinio (NJL) model with three-flavors consists of three terms:

$$\mathcal{L} = \bar{q}(i\gamma_\mu\partial^\mu - m_q + \mu\gamma_0)q + \mathcal{L}^{(4)} + \mathcal{L}^{(6)}, \quad (1)$$

where $q = (u, d, s)^T$ is transpose of the quark field, m_q is a flavor symmetric quark mass ($m_u = m_d = m_s$). $\mathcal{L}^{(4)}$ and $\mathcal{L}^{(6)}$ are the four-fermion interaction and six-fermion interaction, respectively. The standard choice of $\mathcal{L}^{(4)}$ is [5, 6],

$$\mathcal{L}^{(4)} = \mathcal{L}_\chi^{(4)} + \mathcal{L}_d^{(4)}, \quad (2)$$

$$\begin{aligned} \mathcal{L}_\chi^{(4)} &= G \sum_{a=0}^8 [(\bar{q}\tau_a q)^2 + (\bar{q}i\gamma_5\tau_a q)^2] \\ &= 8G\text{tr}(\phi^\dagger\phi), \end{aligned} \quad (3)$$

$$\begin{aligned} \mathcal{L}_d^{(4)} &= H \sum_{A, A'=2,5,7} [(\bar{q}i\gamma_5\tau_A\lambda_{A'}C\bar{q}^T)(q^TCi\gamma_5\tau_A\lambda_{A'}q) \\ &\quad + (\bar{q}\tau_A\lambda_{A'}C\bar{q}^T)(q^TC\tau_A\lambda_{A'}q)] \\ &= 2H\text{tr}[d_L^\dagger d_L + d_R^\dagger d_R], \end{aligned} \quad (4)$$

where $\phi_{ij} \equiv (\bar{q}_R)_a^j(q_L)_a^i$, $(d_L)_{ai} \equiv \epsilon_{abc}\epsilon_{ijk}(q_L)_b^j C(q_L)_c^k$, and $(d_R)_{ai} \equiv \epsilon_{abc}\epsilon_{ijk}(q_R)_b^j C(q_R)_c^k$, with a, b, c and i, j, k the color and flavor indices, and C the charge conjugation operator. tr is taken over the flavor indices. The flavor U(3) generators τ_a ($a = 0, \dots, 8$) are normalized so that $\text{tr}[\tau_a\tau_b] = 2\delta_{ab}$, and τ_A and $\lambda_{A'}$ with $A, A' = 2, 5, 7$ are antisymmetric generators of flavor and SU(3) color, respectively. The coupling constants G and H with dimension $(\text{mass})^{-2}$ are assumed to be positive. Starting from the one-gluon exchange interaction and apply a simple Fierz transformation, we obtain the ratio $H/G = 3/4$. However, we treat G and H as independent parameters of the effective Lagrangian and as detailed in Sec. III take the values common in the literature.

The four-fermion interactions introduced above are invariant under $\text{SU}(3)_L \times \text{SU}(3)_R \times \text{U}(1)_A \times \text{U}(1)_B$ symmetry. The interaction $\mathcal{L}_\chi^{(4)}$ produces attraction of $q\bar{q}$ pairs in the color-singlet and spin-parity 0^\pm channel, inducing dynamical breaking of chiral symmetry with formation of a chiral condensate [38]. Similarly $\mathcal{L}_d^{(4)}$ leads to attraction of qq pairs in the color-anti-triplet and spin-parity 0^\pm channel, inducing color-flavor locked (CFL) superconductivity with formation of a diquark condensate [39].

The six-fermion interaction in our model consists of two parts,

$$\mathcal{L}^{(6)} = \mathcal{L}_\chi^{(6)} + \mathcal{L}_{\chi d}^{(6)}. \quad (5)$$

$\mathcal{L}_\chi^{(6)}$ is the standard Kobayashi-Maskawa-'t Hooft (KMT) interaction [40, 41],

$$\mathcal{L}_\chi^{(6)} = -8K(\det\phi + \text{h.c.}). \quad (6)$$

This interaction, invariant under $SU(3)_L \times SU(3)_R \times U(1)_B$ symmetry but not under $U(1)_A$ symmetry, accounts for the axial anomaly in QCD due to instantons. For positive coupling constant K with dimension $(\text{mass})^{-5}$, as we assume, the η' meson has a larger mass than the other pseudo Nambu-Goldstone bosons (π, η, K) . The term (6) serves the role in the QCD phase structure of making the chiral phase transition first-order as a function of T at $\mu = 0$ for massless three-flavor limit [42].

As pointed out in [17, 18], the instanton couples the diquark condensate and the chiral condensate, which modifies the QCD phase structure in the intermediate density region. The effective interaction between the chiral and diquark pairing fields is described by a six-fermion term,

$$\mathcal{L}_{\chi d}^{(6)} = K' \left(\text{Tr}[(d_R^\dagger d_L)\phi] + \text{h.c.} \right), \quad (7)$$

which has $SU(3)_L \times SU(3)_R \times U(1)_B$ symmetry but breaks $U(1)_A$ symmetry explicitly. It is this term that is responsible for the low temperature critical point. We assume $K' > 0$, so that qq pairs in the positive parity channel, $\langle d_L \rangle = -\langle d_R \rangle$, are energetically favored, as suggested from the weak-coupling instanton calculations [43, 44]. Since the term (7) acts as an external field for χ , it washes out the first-order chiral phase transition at intermediate density for sufficiently large $K'|\langle d_R \rangle|^2$ [17, 18]. If we start from the instanton vertex and apply a simple Fierz transformation, we obtain the ratio $K'/K = 1$. However, since there is no a priori reason that K and K' have this ratio in the effective Lagrangian level, we keep them as independent parameters.

The favorable condensates by the interaction $\mathcal{L}^{(4)} + \mathcal{L}^{(6)}$ are the flavor-symmetric chiral and diquark condensates in the spin-parity 0^+ channel, defined by

$$\chi \delta_{ij} = \langle \bar{q}_a^i q_a^j \rangle, \quad (8)$$

$$s \delta_{AA'} = \langle q^T C \gamma_5 \tau_A \lambda_{A'} q \rangle. \quad (9)$$

Here the condensate order parameters χ and s , which are proportional to the order parameters σ and d defined in the previous Ginzburg-Landau analysis [17, 18], are related to the parameters ϕ and $d_{L,R}$ defined below Eq. (4) by

$$\chi \delta_{ij} = 2 \langle \phi_{ij} \rangle, \quad (10)$$

$$s \delta_{ai} = 2 \langle (d_L)_{ai} \rangle = -2 \langle (d_R)_{ai} \rangle. \quad (11)$$

We work at the mean-field level, linearizing the the products of operators X and Y as $X^2 \rightarrow 2\langle X \rangle X - \langle X \rangle^2$, $XY \rightarrow \langle X \rangle Y + \langle Y \rangle X - \langle X \rangle \langle Y \rangle$, and $X^2 Y \rightarrow \langle X \rangle^2 Y + 2\langle X \rangle \langle Y \rangle X - 2\langle X \rangle^2 \langle Y \rangle$. Subtraction of the constant terms avoids double counting the interactions. In mean-field deviations from factorization are partially compensated for by redefinition of the coupling constants G , H ,

K , and K' . Then $\mathcal{L}^{(4)}$ and $\mathcal{L}^{(6)}$ reduce to

$$\begin{aligned} \mathcal{L}_\chi^{(4)} &\rightarrow 4G\chi\bar{q}q - 6G\chi^2, \\ \mathcal{L}_d^{(4)} &\rightarrow H [s^*(q^T C \gamma_5 \tau_A \lambda_A q) + \text{h.c.}] - 3H|s|^2, \\ \mathcal{L}_\chi^{(6)} &\rightarrow -2K\chi^2\bar{q}q + 4K\chi^3, \\ \mathcal{L}_{\chi d}^{(6)} &\rightarrow -\frac{K'}{4}|s|^2\bar{q}q - \frac{K'}{4}\chi [s^*(q^T C \gamma_5 \tau_A \lambda_A q) + \text{h.c.}] \\ &\quad + \frac{3K'}{2}|s|^2\chi. \end{aligned} \quad (12)$$

Here and below we implicitly sum over $A = 2, 5, 7$ unless otherwise stated.

To derive the thermodynamic potential, it is most convenient to work in the Nambu-Gor'kov formalism; we introduce the bispinor field

$$\Psi = \frac{1}{\sqrt{2}}(q, q^C)^T, \quad (13)$$

with $q^C = C\bar{q}^T$ (and $\bar{q}^C = q^T C$) the charge-conjugate quark field. Then the linearized form of the NJL Lagrangian becomes

$$\mathcal{L} = \bar{\Psi} S^{-1} \Psi - U. \quad (14)$$

Here $S^{-1}(p)$ is the inverse propagator in the momentum space:

$$S^{-1}(p) = \begin{pmatrix} \gamma_\mu p^\mu + \mu\gamma_0 - M & \Delta\gamma_5\tau_A\lambda_A \\ -\Delta^*\gamma_5\tau_A\lambda_A & \gamma_\mu p^\mu - \mu\gamma_0 - M \end{pmatrix}, \quad (15)$$

where the dynamical Dirac mass in the $q\bar{q}$ -channel reads

$$M(\chi, s, m_q) = m_q - 4 \left(G - \frac{1}{8}K\chi \right) \chi + \frac{1}{4}K'|s|^2, \quad (16)$$

and the dynamical Majorana mass in the qq -channel reads

$$\Delta(\chi, s) = -2 \left(H - \frac{1}{4}K'\chi \right) s. \quad (17)$$

They are both dependent on the order parameters, χ and s . The constant term needed to subtract double counting of the interactions in \mathcal{L} is

$$U(\chi, s) = 6G\chi^2 + 3H|s|^2 - 4K\chi^3 - \frac{3}{2}K'|s|^2\chi. \quad (18)$$

The terms in Eqs. (16), (17), and (18) are shown diagrammatically in Figs. 2(a)-(d), 3(a)-(b), and 4(a)-(d), respectively. The chiral-diquark coupling (the K' -term) enhances the attractions in both the $\bar{q}q$ and qq channels.

The thermodynamic potential at temperature T and quark chemical potential μ is given by

$$\Omega = -T \sum_n \int \frac{d^3p}{(2\pi)^3} \frac{1}{2} \text{Tr} \ln \left[\frac{1}{T} S^{-1}(i\omega_n, \vec{p}) \right] + U(\chi, s), \quad (19)$$

where Tr is taken over the bispinor space with the factor $1/2$ in front to correct for double counting of degrees of freedom. Evaluating the trace and summing over the

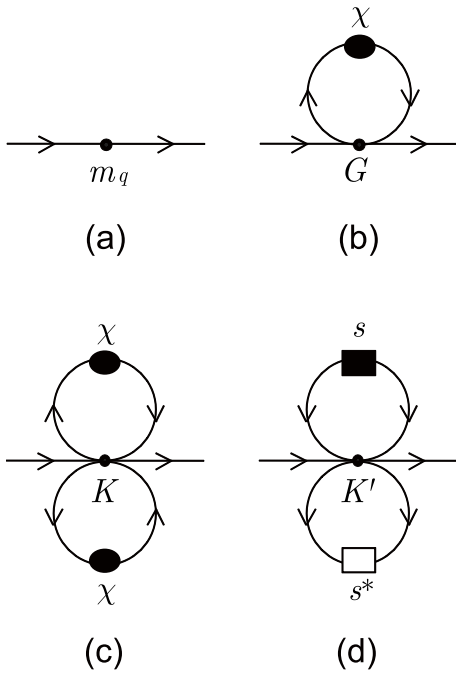


FIG. 2. Four contributions to the Dirac mass M (constituent quark mass). The chiral condensate χ is denoted by a black circle, the diquark condensate s by a black square, and s^* by a white square.

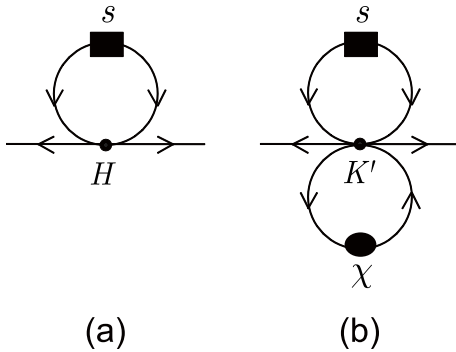


FIG. 3. Two contributions to the Majorana mass Δ (superconducting gap).

fermionic Matsubara frequencies $p^0 = i\omega_n = (2n+1)\pi iT$, we arrive at the thermodynamic potential [6]:

$$\Omega = - \int \frac{d^3 p}{(2\pi)^3} \sum_{\pm} \left\{ \left[16T \ln(1 + e^{-\omega_8^{\pm}/T}) + 8\omega_8^{\pm} \right] + \left[2T \ln(1 + e^{-\omega_1^{\pm}/T}) + \omega_1^{\pm} \right] \right\} + U(\chi, s), \quad (20)$$

where

$$\omega_8^{\pm} = \sqrt{(E_p \pm \mu)^2 + \Delta_1^2}, \quad (21)$$

$$\omega_1^{\pm} = \sqrt{(E_p \pm \mu)^2 + \Delta_8^2}, \quad (22)$$

are the dispersion relations for the quasi-quarks in the octet and singlet representations, with $E_p = \sqrt{p^2 + M^2}$,

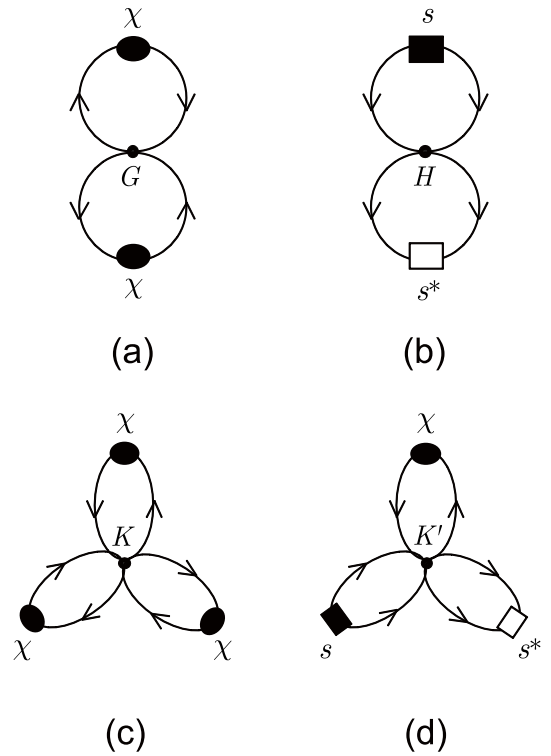


FIG. 4. Four contributions to the constant term U .

$\Delta_1 = 2\Delta$, and $\Delta_8 = \Delta$. Equations (16) and (20) imply that $\chi < 0$ is energetically favored for non-zero m_q . On the other hand, s is generally complex and the thermodynamic potential is a function of $|s|^2$.

III. PHASE STRUCTURE

We now explore the effect of the attractive K' -term induced by the axial anomaly on the phase structure in the (μ, T) -plane of the three-flavor NJL model. The phase structures can be determined numerically by looking for the values of χ and s that minimize the thermodynamic potential in Eq. (20) globally. We follow the parameter choice of [6] where the coupling constants G and K are chosen to fit empirical mesonic quantities and the chiral condensate in the QCD vacuum. Table I shows two sets of parameters we adopt below. We vary the strength of the chiral-diquark coupling (the K' term) by hand. In order to illustrate how the anomaly changes the conventional phase structure and to avoid the complications of charge neutrality and β -equilibrium, we assume SU(3) flavor symmetry, $m_u = m_d = m_s \equiv m_q$.

A. Without the chiral-diquark interplay

We first show the phase structures without the K' -term in Fig. 5. Panels (a) and (b) show the results of the case of massless quarks, I, and finite mass quarks,

	m_q [MeV]	$G\Lambda^2$	$H\Lambda^2$	$K\Lambda^5$	M [MeV]	$\chi^{1/3}$ [MeV]
I	0	1.926	1.74	12.36	355.2	-240.4
II	5.5	1.918	1.74	12.36	367.6	-241.9

TABLE I. Two sets of parameters in the present three-flavor NJL model: the current quark mass m_q , coupling constants G , H , and K , with a spatial momentum cutoff $\Lambda = 602.3$ MeV [6]. The dynamical quark mass M and the chiral condensate χ in the vacuum are also given.

II, respectively. The phase diagram contains of a normal (NOR) phase defined by $\chi = s = 0$, a Nambu-Goldstone (NG) phase defined by $\chi \neq 0$ and $s = 0$, and a color superconducting (CSC) phase defined by $\chi = 0$ and $s \neq 0$.¹ The chiral phase transition between the NG and NOR (or NG and CSC) phases is first-order, with the chiral condensate χ changing discontinuously, while the color superconducting phase transition between the CSC and NOR phases is second-order, with the diquark condensate s changing continuously but not smoothly with a discontinuity in the diquark susceptibility $\partial s/\partial T$.

In case II, the current quark mass changes first-order chiral phase transition to a crossover at high temperature, whereas the first-order transition at high density region still remains, as shown in Fig. 5(b). As a result, the second-order critical point, the Asakawa-Yazaki point [14, 15], appears in the (μ, T) -plane. The QCD critical point moves down towards the μ -axis with increasing quark mass m_q . The region $\chi \sim 0$ is characterized by explicit breaking of chiral symmetry by the quark mass, while in the region $\chi \neq 0$, chiral symmetry is dynamically broken.

B. With the chiral-diquark interplay

When the strength of the chiral-diquark coupling due to axial anomaly, K' , is relatively small ($K' < 4.1K$ in case I and $K' < 3.8K$ in case II), the topologies of the phase structures remain unchanged, as one sees in Figs. 5(a) and (b). On the other hand, once K' exceeds a critical value K'_c , the topological structure of the phase diagram changes as seen in Fig. 6 (shown for $K' = 4.2K$): as discussed in [17, 18] using the Ginzburg-Landau approach, the K' -term, which acts as an external field for χ , turns the first-order chiral phase transition into a crossover, and leads to a low T critical point at intermediate density. As a result, the coexistence (COE) phase defined by $\chi \neq 0$ and $s \neq 0$ spreads over the higher density region across the second-order phase boundary from the NG phase in both cases I and II. The emergence of the COE phase is consistent with the model-independent

¹ Even when chiral symmetry is broken only slightly ($\chi \sim 0$) by the current quark mass, we use the same classification in terms of NOR, NG and COE as in Fig. 5(b).

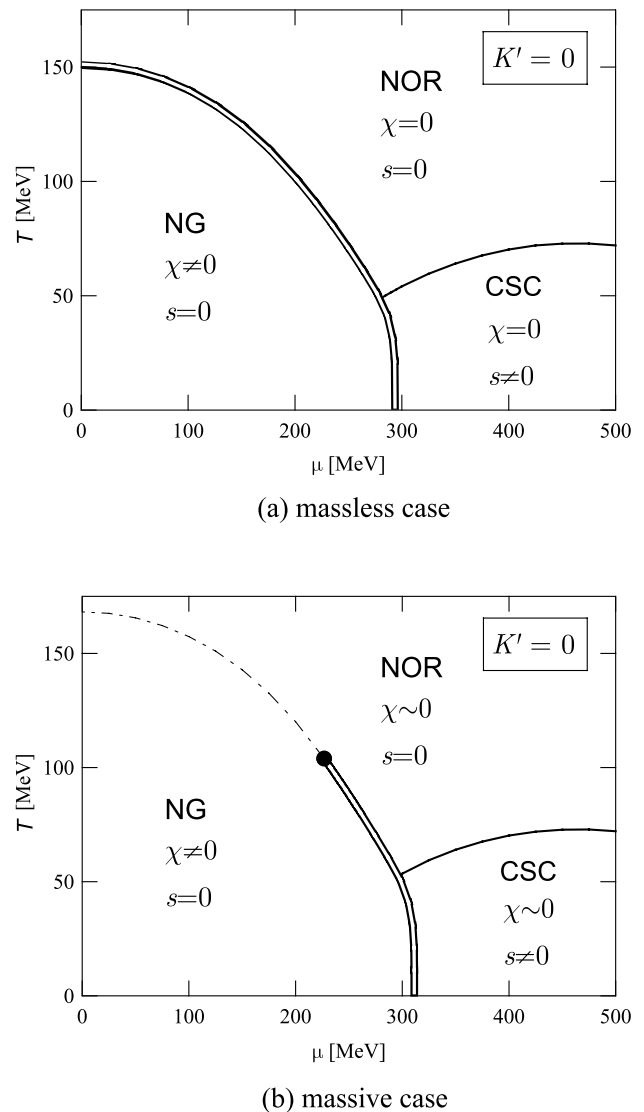
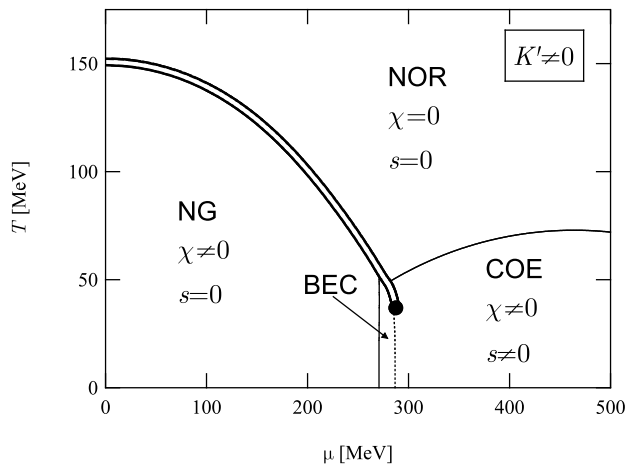


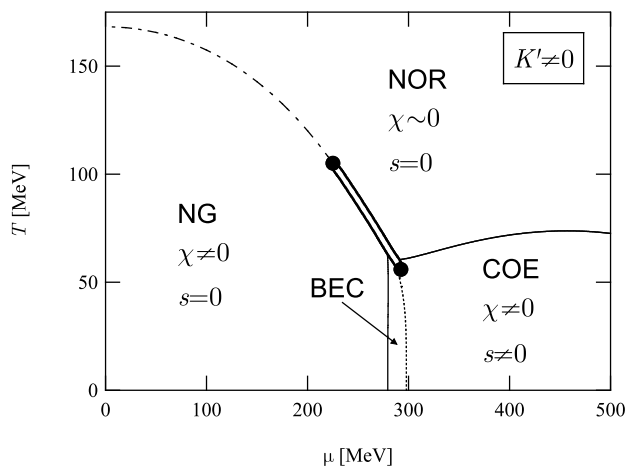
FIG. 5. The phase structure in the (μ, T) -plane in the three-flavor NJL model without the axial anomaly for (a) case I, massless quarks, and (b) case II, finite mass quarks. Phase boundaries with a second-order transition are denoted by a single line and a first-order transition by a double line. The dashed-dot line at high T in panel (b) shows the effective chiral crossover line, at which the susceptibility $\partial\chi/\partial T$ peaks. See the text for further detail.

result that the chiral condensate χ is proportional to the instanton density (or the strength of the axial anomaly) in the CFL phase [44].

In Fig. 7, we depict K'_c as a function of K for several values of the current quark mass, $m_q = 0$, $m_q = 5.5$ MeV, and $m_q = 140.7$ MeV. The K'_c -line separates the crossover and first-order regions; the chiral-diquark coupling K' favors the crossover, while the triple chiral coupling K favors first-order. As m_q increases, the crossover region is enlarged since the current quark mass acts as an external field on the chiral condensate, weakening the



(a) massless case



(b) massive case

FIG. 6. Phase structure in the (μ, T) -plane in the three-flavor NJL model with the axial anomaly for (a) massless quarks, and (b) finite mass quarks. The phase boundaries with a second-order transition are denoted by a single line and a first-order transition by a double line. The BEC-BCS crossover (dotted) line in (a) and (b) is defined by $\mu = M(\mu, T)$, the dynamical quark mass.

chiral transition.

IV. BEC-BCS CROSSOVER INDUCED BY THE AXIAL ANOMALY

The axial anomaly, for sufficiently large chiral-diquark coupling K' , not only triggers the low T critical point, but also a BEC-BCS crossover in the COE phase, as discussed in [37] in qualitative analogy with the cold atomic gases in condensed-matter physics. Physically the BEC regime is characterized by quark-pair sizes small compared to the interparticle spacing, while in the BCS regime the pair size is large compared with the interparti-

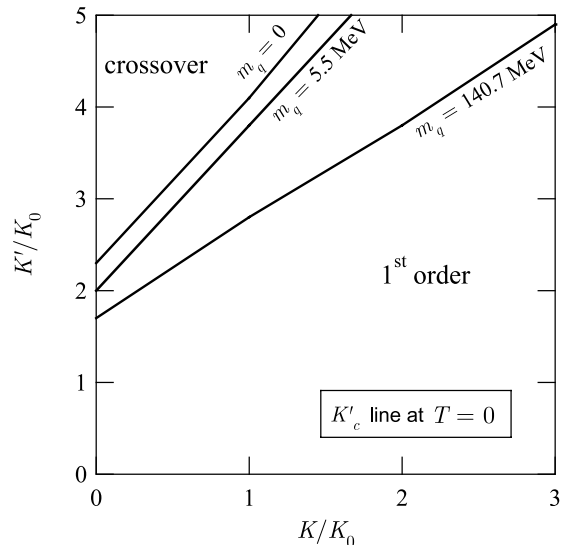


FIG. 7. Critical lines in the (K, K') -plane at $T = 0$ for several values of the current quark mass m_q ($K_0\Lambda^5 \equiv 12.36$). Chiral phase transition is realized as a smooth crossover in the region above the corresponding line while it is of first-order below the line.

cle spacing. The possibility of a BEC-BCS crossover in a color superconductor, and the presence of a BEC regime, was first pointed out in [28] by looking at the change in size of the pairs with density. As shown later within an NJL-type model such a BEC regime appears for sufficiently large pairing attraction, H , in the qq -channel [35]. The novel feature we stress here is that the axial anomaly helps to realize the BEC regime through its contribution to the effective qq coupling in (17),

$$H' \equiv H + \frac{1}{4}K'|\chi|. \quad (23)$$

Although $H \simeq 0.9G$ alone is not enough to produce the diquark BEC (see Fig. 5), the chiral-diquark coupling K' increases H' sufficiently for a BEC to develop (see Fig. 6).

Analytically, the distinction between the BEC and BCS regimes lies in the nature of the quasiparticle dispersion relations, Eqs. (21) and (22). For $\mu > M$, the minima of the dispersion relations are at nonzero momentum $p = \sqrt{\mu^2 - M^2}$, with excitation gaps Δ_1 and Δ_8 , a structure characteristic of the BCS regime. On the other hand, for $\mu < M$, the minima of the dispersion curves are at $p = 0$, a structure characteristic of the BEC regime [26]. Figures 6 (a) and (b) show the curve $\mu = M(\mu, T)$ as the dotted line in the COE region. A BEC of bound diquarks exists between the solid and dotted lines. (Note that at $T = 0$ the dotted line ends at $\mu = 286.6$ MeV in case I and at $\mu = 297.8$ MeV in case II, reflecting the decrease of $M(\mu, T = 0)$ from its vacuum value, Table I.)

The structure of the crossover from BEC to BCS, at the NG-BEC and NOR-COE boundaries in Figure 6, is most clearly defined in terms of the diquark correlation

function

$$G_D(\tau, \mathbf{x}) \equiv -4H^2 \langle T_\tau [s_A(\tau, \mathbf{x}) s_A^\dagger(0, \mathbf{0})] \rangle, \quad (24)$$

with $s_A(\tau, \mathbf{x}) = q^T(\tau, \mathbf{x}) C \gamma_5 \tau_A \lambda_A q(\tau, \mathbf{x})$ (no summation over A). In the random phase approximation (RPA), this correlation function in the complex frequency (z) plane at temperatures above the diquark condensation temperature T_c is given by

$$G_D^{-1}(z, \mathbf{q} = \mathbf{0}) = \frac{1}{4H'} - 4 \sum_{\mp} \int_{p \leq \Lambda} \frac{d^3 p}{(2\pi)^3} \frac{1 - 2f(E_p \mp \mu)}{2(E_p \mp \mu) \mp z}, \quad (25)$$

where $f(\epsilon) = 1/(e^{\epsilon/T} + 1)$ is the Fermi distribution function and Λ is the ultraviolet cutoff. As we see from Eq. (25), G_D has a branch cut on the real axis for $z \geq 2(M - \mu)$ (as well as a branch cut for $z \leq -2(M + \mu)$ from the antiparticle contribution).

In the regime $\mu < M(\mu, T)$, for sufficiently large H' , $G_D(z, \mathbf{0})$ has a pole on the real frequency axis for $0 \leq z = M_D(\mu, T) - 2\mu \leq 2(M - \mu)$, with $M_D(\mu, T)$ the mass of a bound diquark. The system undergoes a BEC condensation when, at a given temperature, this pole first reaches zero frequency, $G_D^{-1}(0, \mathbf{0}) = 0$ [27, 29, 45]; thus the condition

$$2\mu = M_D(\mu, T), \quad (26)$$

determines the NG-BEC boundary (Fig. 6). With increasing μ the branch cut starting at $2(M - \mu)$ eventually reaches down to $z = 0$, at which point the pole at the origin begins to move to complex values in the second Riemann sheet. For $\mu > M(\mu, T)$, the condition $G_D^{-1}(0, \mathbf{0}) = 0$ defines the onset of BCS pairing, studied in detail in Ref. [46], and determines the NOR-COE boundary (Fig. 6).

Due to the abrupt change of χ across the first-order transition line, the NG-BEC and NOR-COE boundaries are not smoothly connected; the former touches the first-order line at higher temperature than the latter (see Fig. 6). As discussed more fully in [18], this difference can be understood by noting that a larger chiral condensate χ reduces the density of states at the Fermi surface and simultaneously increases the effective qq coupling H' [see Eq. (23)]. Since the latter effect dominates in the present parameter set, the critical temperature for diquark pairing is larger on the left side of the double line.

The behavior of the Dirac mass M , the Majorana mass or gap Δ , and the bound diquark mass M_D associated with the phase diagram in Fig. 6(b), are plotted in Fig. 8 as functions of μ for three temperatures, $T=0, 62, \text{ and } 80$ MeV. At zero temperature, we see the successive transitions from the NG phase, the BEC regime in the COE phase, to the BCS regime in the COE phase, with increasing μ . The onset of BEC at $\mu = 279.2$ MeV is determined by the condition $M_D - 2\mu = 0$. For $T = 62$ MeV, we see rather the successive transitions from the NG phase, the BEC regime in the COE phase, the NOR phase, to the BCS regime in the COE phase, with increasing μ . The transition from the BEC regime in the COE phase to the

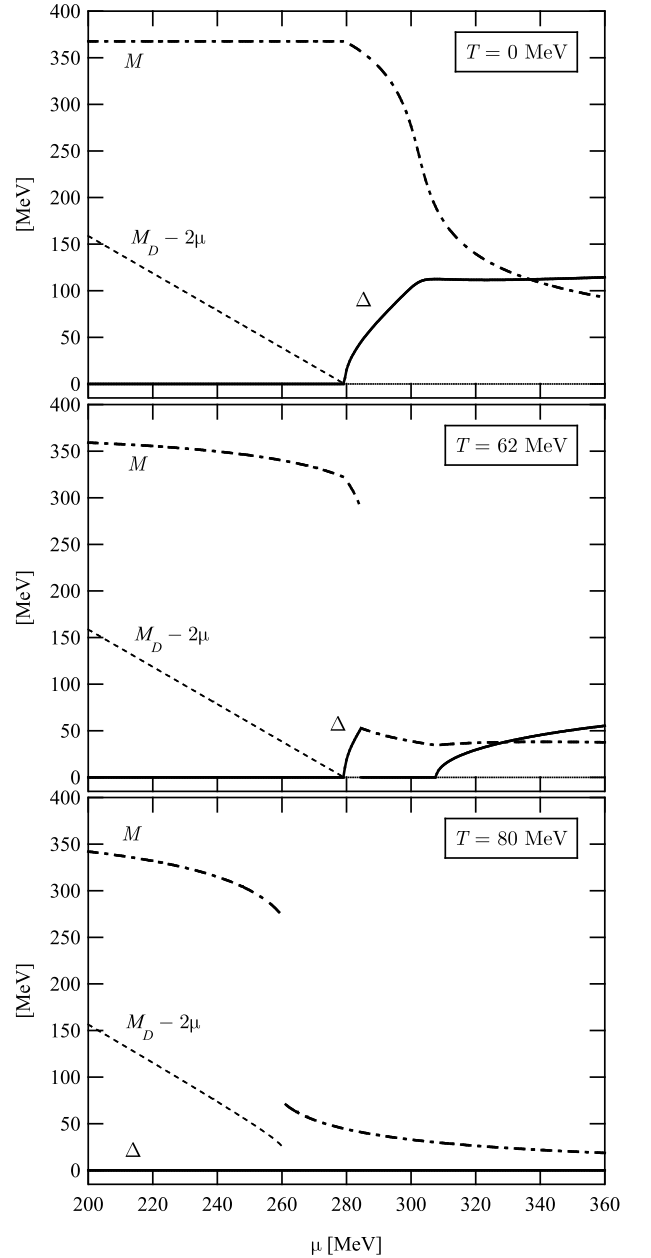


FIG. 8. The Dirac mass (M) and the Majorana mass (Δ) as functions of μ for $T = 0$ MeV (top), 62 MeV (middle), and 80 MeV (bottom). The excitation gap of the bound diquark in the medium, $M_D - 2\mu$, extracted from the isolated zero of Eq. (25), is also shown. The parameters are the same as in Fig. 6(b).

NOR phase is first-order at $\mu = 284.5$ MeV, with both M and Δ jumping discontinuously. The two phase transitions, from the NG phase to the BEC regime in the COE phase, and from the NOR phase to the BCS regime in the COE phase, signal the onset of a non-zero Majorana mass. Both transitions are correctly described in terms of the diquark correlation function [see Eq. (25)]. For $T = 80$ MeV, the system undergoes a first-order transi-

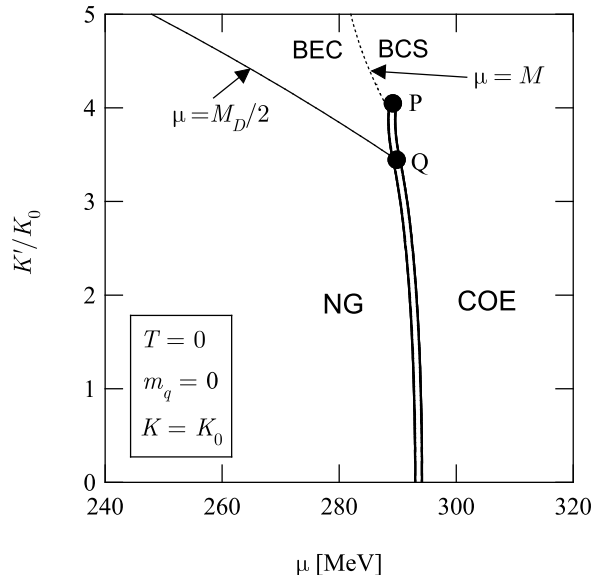


FIG. 9. The phase diagram in the (μ, K') -plane at $T = 0$ for massless quarks, with the NG and COE phases. The BEC-BCS crossover in the COE phase for large K' is shown as a dotted line. The critical point and the critical end point are denoted by P and Q, respectively.

tion, from the NG phase to the NOR phase at $\mu = 260.7$ MeV, which takes place before bound diquarks start to condense.

Finally we consider the effect of the chiral-diquark coupling K' on the phases at $T = 0$. Figure 9 shows the phase diagram in the (μ, K') -plane for massless quarks. (A similar structure holds for finite mass quarks.) For small K' , the system has an NG phase and a COE phase separated by a first-order line indicated by the double line which eventually terminates for large K' at the critical point P. On the other hand, for K' sufficiently large compared with the cubic coupling, K , of the chiral field, a BEC regime of bound diquarks appears across a second-order phase transition (solid line) from the NG phase at a critical chemical potential $\mu = M_D/2$; the phase boundary joins the first-order line at the critical end point Q. The dotted line, $\mu = M(\mu, T)$, shows the BEC-BCS crossover; for somewhat smaller K' , a novel first-order transition from the BEC to BCS regimes appears between P and Q, with discontinuous changes of both the chiral and diquark condensates.

V. DISCUSSION

We have explored here the phase structure of dense three-flavor matter using the Nambu–Jona-Lasinio model incorporating the attraction between the chiral and di-

quark condensates induced by the axial anomaly. We demonstrated that the low temperature critical point between the hadronic phase and the color superconducting phase predicted by the previous Ginzburg-Landau analysis [17, 18] indeed appears in the phase diagram for sufficiently large chiral-diquark coupling. We have also shown in Eq. (23) that the axial anomaly enhances the attractive interaction between quarks, leading to the emergence of a Bose-Einstein condensate (BEC) of diquark molecules. As a result, a BEC-BCS crossover in the diquark pairing appears in the coexistence phase, which has both non-zero chiral and diquark condensates.

In the phase diagram of the NJL model derived here, the BEC regime is realized adjacent to the lower density Nambu-Goldstone phase of massive quarks. In QCD, however, the low density phase is in reality nuclear matter; There remains the important problem of learning how the gas of bound diquarks and unpaired quarks undergoes a transition to a gas of three-quark bound states, or nucleons, at low density. Describing this transition will require going beyond the mean-field approximation, and RPA, to take into account residual interactions between the diquarks and unpaired quarks. Recent work [47, 48] on mixtures of bosonic and fermionic atoms indicates a phase diagram very reminiscent of this scenario in QCD.

It is also important to make our phase diagram more realistic by including effects such as the Fermi momentum mismatch induced by a strange quark mass, charge neutrality and β -equilibrium. Open questions include whether the low temperature critical point can survive in an inhomogeneous chiral crystalline phase [49, 50] or the Fulde-Ferrell-Larkin-Ovchinnikov phase [51–56], and how the phase structure obtained here is affected by the confinement-deconfinement phase transition characterized by the Polyakov loop [7–10]. We defer these problems to future publications.

ACKNOWLEDGMENTS

We would like to thank S. Rössner and W. Weise for useful discussions. A part of numerical calculations was carried out on Altix3700 BX2 at YITP in Kyoto University. The work of GB was supported in part by NSF Grant No. PHY07-01611; he also thanks the G-COE program of the Physics Department of the University of Tokyo for hospitality and support during the completion of this work. TH was supported in part by the Grant-in-Aid for Scientific Research on Innovative Areas (No. 2004: 20105003). NY is supported by the Japan Society for the Promotion of Science for Young Scientists.

-
- [1] M. G. Alford, A. Schmitt, K. Rajagopal, and T. Schäfer, *Rev. Mod. Phys.* **80**, 1455 (2008).
- [2] K. Yagi, T. Hatsuda, and Y. Miake, *Quark-gluon plasma: From big bang to little bang* (Camb. Monogr. Part. Phys. Nucl. Phys. Cosmol., 2005).
- [3] Y. Aoki *et al.*, *JHEP* **06**, 088 (2009).
- [4] A. Bazavov *et al.*, *Phys. Rev.* **D80**, 014504 (2009).
- [5] T. Hatsuda and T. Kunihiro, *Phys. Rept.* **247**, 221 (1994).
- [6] M. Buballa, *Phys. Rept.* **407**, 205 (2005).
- [7] K. Fukushima, *Phys. Lett.* **B591**, 277 (2004); *Phys. Rev.* **D77**, 114028 (2008).
- [8] C. Ratti, M. A. Thaler, and W. Weise, *Phys. Rev.* **D73**, 014019 (2006).
- [9] S. Rössner, C. Ratti, and W. Weise, *Phys. Rev.* **D75**, 034007 (2007).
- [10] T. Hell, S. Rössner, M. Cristoforetti, and W. Weise, *Phys. Rev.* **D79**, 014022 (2009).
- [11] A. M. Halasz, A. D. Jackson, R. E. Shrock, M. A. Stephanov, and J. J. M. Verbaarschot, *Phys. Rev.* **D58**, 096007 (1998).
- [12] B. Vanderheyden and A. D. Jackson, *Phys. Rev.* **D62**, 094010 (2000).
- [13] T. Sano, H. Fujii, and M. Ohtani, *Phys. Rev.* **D80**, 034007 (2009).
- [14] M. Asakawa and K. Yazaki, *Nucl. Phys.* **A504**, 668 (1989).
- [15] A. Barducci, R. Casalbuoni, S. De Curtis, R. Gatto, and G. Pettini, *Phys. Lett.* **B231**, 463 (1989).
- [16] P. de Forcrand and O. Philipsen, *JHEP* **11**, 012 (2008).
- [17] T. Hatsuda, M. Tachibana, N. Yamamoto, and G. Baym, *Phys. Rev. Lett.* **97**, 122001 (2006).
- [18] N. Yamamoto, M. Tachibana, T. Hatsuda, and G. Baym, *Phys. Rev.* **D76**, 074001 (2007).
- [19] T. Schäfer and F. Wilczek, *Phys. Rev. Lett.* **82**, 3956 (1999).
- [20] T. Hatsuda, M. Tachibana, and N. Yamamoto, *Phys. Rev.* **D78**, 011501 (2008).
- [21] N. Yamamoto and T. Kanazawa, *Phys. Rev. Lett.* **103**, 032001 (2009).
- [22] M. Kitazawa, T. Koide, T. Kunihiro, and Y. Nemoto, *Prog. Theor. Phys.* **108**, 929 (2002); **110**, 185 (2003).
- [23] Z. Zhang, K. Fukushima, and T. Kunihiro, *Phys. Rev.* **D79**, 014004 (2009).
- [24] Z. Zhang and T. Kunihiro, *Phys. Rev.* **D80**, 014015 (2009).
- [25] D. M. Eagles, *Phys. Rev.* **186**, 456 (1969).
- [26] A. J. Leggett, *J. Phys. C* **41**, 7 (1980).
- [27] P. Nozières and S. Schmitt-Rink, *J. Low. Temp. Phys.* **59**, 195 (1985).
- [28] H. Abuki, T. Hatsuda, and K. Itakura, *Phys. Rev.* **D65**, 074014 (2002).
- [29] Y. Nishida and H. Abuki, *Phys. Rev.* **D72**, 096004 (2005).
- [30] K. Nawa, E. Nakano, and H. Yabu, *Phys. Rev.* **D74**, 034017 (2006).
- [31] H. Abuki, *Nucl. Phys.* **A791**, 117 (2007).
- [32] J. Deng, A. Schmitt, and Q. Wang, *Phys. Rev.* **D76**, 034013 (2007).
- [33] G.F. Sun, L. He, and P. Zhuang, *Phys. Rev.* **D75** 096004 (2007).
- [34] L. He and P. Zhuang, *Phys. Rev.* **D76**, 056003 (2007).
- [35] M. Kitazawa, D. H. Rischke, and I. A. Shovkovy, *Phys. Lett.* **B663**, 228 (2008).
- [36] T. Brauner, *Phys. Rev. D* **77**, 096006 (2008).
- [37] G. Baym, T. Hatsuda, M. Tachibana, and N. Yamamoto, *J. Phys.* **G35**, 104021 (2008).
- [38] Y. Nambu and G. Jona-Lasinio, *Phys. Rev.* **122**, 345 (1961); **124**, 246 (1961).
- [39] M. G. Alford, K. Rajagopal, and F. Wilczek, *Nucl. Phys.* **B537**, 443 (1999).
- [40] M. Kobayashi and T. Maskawa, *Prog. Theor. Phys.* **44**, 1422 (1970).
- [41] G. 't Hooft, *Phys. Rev. Lett.* **37**, 8 (1976); *Phys. Rev.* **D14**, 3432 (1976).
- [42] R. D. Pisarski and F. Wilczek, *Phys. Rev.* **D29**, 338 (1984).
- [43] T. Schäfer, *Phys. Rev.* **D65**, 094033 (2002).
- [44] N. Yamamoto, *JHEP* **12**, 060 (2008).
- [45] G. Baym, J.-P. Blaizot, M. Holzmann, F. Laloë, and D. Vautherin, *Phys. Rev. Lett.* **83**, 1703 (1999).
- [46] M. Kitazawa, T. Koide, T. Kunihiro and Y. Nemoto, *Phys. Rev. D* **65**, 091504 (2002).
- [47] K. Maeda, G. Baym, and T. Hatsuda, *Phys. Rev. Lett.* **103**, 085301 (2009).
- [48] T. Hatsuda and K. Maeda, arXiv:0912.1437 [hep-ph].
- [49] E. Nakano and T. Tatsumi, *Phys. Rev.* **D71**, 114006 (2005).
- [50] D. Nickel, *Phys. Rev. Lett.* **103**, 072301 (2009).
- [51] M. G. Alford, J. A. Bowers, and K. Rajagopal, *Phys. Rev.* **D63**, 074016 (2001).
- [52] J. A. Bowers and K. Rajagopal, *Phys. Rev.* **D66**, 065002 (2002).
- [53] R. Casalbuoni, R. Gatto, N. Ippolito, G. Nardulli, and M. Ruggieri, *Phys. Lett.* **B627**, 89 (2005).
- [54] M. Mannarelli, K. Rajagopal, and R. Sharma, *Phys. Rev.* **D73**, 114012 (2006).
- [55] K. Rajagopal and R. Sharma, *Phys. Rev.* **D74**, 094019 (2006).
- [56] D. Nickel and M. Buballa, *Phys. Rev.* **D79**, 054009 (2009).